JOURNAL OF SOLID STATE CHEMISTRY **124,** 278–286 (1996)
ARTICLE NO. 0237

A HREM Study on $La_{1/3}Sr_{2/3}FeO_{3-y}$, I: ($0 \leq y \leq 0.10$)

E. García-González,* M. Parras,* J. M. González-Calbet,*,[1] and M. Vallet-Regí†

*Dpto. Química Inorgánica, Facultad de Químicas, Universidad Complutense, 28040-Madrid, Spain; and †Dpto. Química Inorgánica y Bioinorgánica, Facultad de Farmacia, Universidad Complutense, 28040-Madrid, Spain

Received November 20, 1995; in revised form April 1, 1996; accepted April 2, 1996

The microstructural study of the $La_{1/3}Sr_{2/3}FeO_{3-y}$ system by electron diffraction and microscopy shows that for the $y = 0.1$ composition, La and Sr are ordered in small domains preserving the 1:2 ratio and following a sinusoidal modulation. This ordered state disappears when no oxygen vacancies are present ($y = 0$), the material presenting a small rhombohedral distortion. © 1996 Academic Press, Inc.

INTRODUCTION

We have recently reported a study on the accommodation of compositional variations in $Ln_{1/3}Ba_{2/3}FeO_{3-y}$ perovskite related materials (Ln = Nd, Sm, Eu, Dy, and Ho) (1–3). The anionic composition was found to be related to the lanthanide element introduced in the A sublattice at some fixed synthesis conditions. Various structural models consisting on different stacking sequences of 6- and 5-coordination layers were proposed, according to the ability of iron to adopt different coordination polyhedra.

Such a coordination for iron varies when changing the earth-alkaline element. Thus, structural studies corresponding to $LaCa_2Fe_3O_z$ (4–6) clearly state that octahedral and tetrahedral coordination are the most stable environment for iron in these materials.

The perovskite series $La_{1-x}Sr_xFeO_{3-\delta}$ ($0 \leq x \leq 1$) was first studied by Waugh (7) who observed complex phase changes from orthorhombic to rhombohedral as a function of x. Since the distortions were very small, no further structural information was obtained. An extensive range of composition in this system has been recently studied in a sistematic way by Dann *et al.* (8), by X-ray diffraction, and Mössbauer spectroscopy. The most recent study on $LaSr_2Fe_3O_{9-y}$ ($0 < y \leq 1$) was performed by Battle *et al.* (9, 10), the materials being characterized by powder neutron diffraction and Mössbauer spectroscopy. The crystal structure of $LaSr_2Fe_3O_8$ was described, as its Ca homologous, as formed by two octahedral layers alternating in an ordered way with one tetrahedral layer along the b axis. For the $LaSr_2Fe_3O_{8.5}$ ($La_{1/3}Sr_{2/3}FeO_{2.83}$) composition, an intuitive structural model consisting on the alternance of 5-coordinated sites separated by two layers of iron in octahedral sites was suggested (10).

The crystal structure of $LaSr_2Fe_3O_{8.94}$ ($Ln_{1/3}Sr_{2/3}FeO_{2.98}$) at room temperature was found to be that of a rhombohedrally distorted perovskite (11). The apparent 2:1 ordering of two types of Fe cations (Fe^{3+} and Fe^{5+}) in the magnetic structure was not accompanied by structural distortion probably due, as they suggest, to the disordered arrangement of Sr and La.

According to the complex problem involving the microstructural aspects of these compounds, we have carried out a study on the accommodation of compositional variations in $Ln_{1/3}Sr_{2/3}FeO_{3-y}$ (Ln = La, Nd, Sm, Gd, and Er). The results we present here concern $La_{1/3}Sr_{2/3}FeO_{3-y}$ for $y = 0$ and $y = 0.1$. Microstructural characterization by means of selected area electron diffraction (SAED) and high resolution electron microscopy (HREM) has enabled us to go deeper inside in the description of these phases.

EXPERIMENTAL

The sample of nominal composition $La_{1/3}Sr_{2/3}FeO_{2.90}$ was prepared by heating stoichiometric amounts of $SrCO_3$, La_2O_3, and α-Fe_2O_3 of annalar quality at 1300°C for 96 h in air. The homogeneous black product obtained was quenched to room temperature in the platinum crucibles used for synthesis.

The former material was used as precursor to obtain the highly oxidized composition $La_{1/3}Sr_{2/3}FeO_{3.00}$, by heating at 800°C (150 bar O_2 pressure) for 12 h. Both chemical analysis and thermogravimetry were used to determine the oxidation state of iron. The average cationic composition was established by inductive coupling plasma (ICP). In both cases, the average cationic composition nicely coincides with the nominal composition.

Powder X-ray diffraction (XRD) was performed on a Siemens D-5000 diffractometer with a graphite monochromator and using Cu$K\alpha$ radiation. SAED was carried out on a JEOL 2000FX electron microscope, fitted with a double tilting goniometer stage (± 45°). HREM was performed

[1] To whom correspondence should be addressed.

0022-4596/96 $18.00

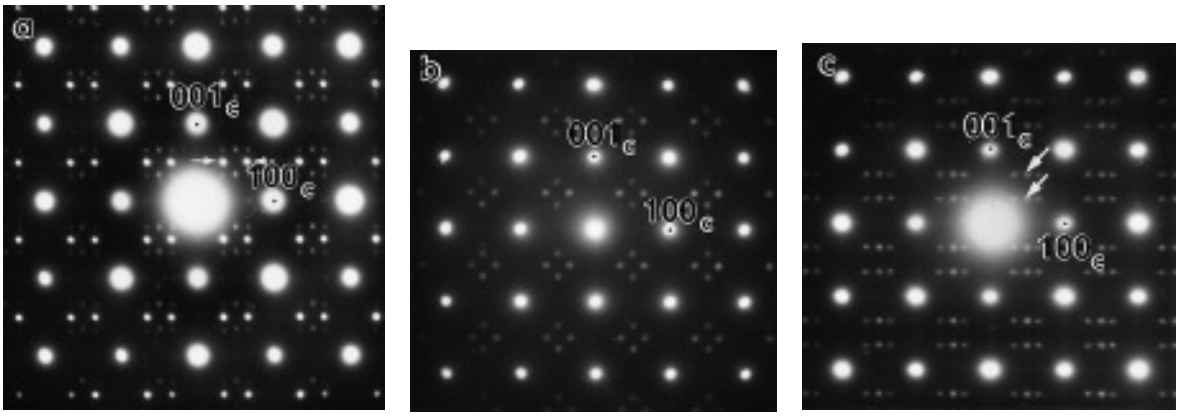

FIG. 1. (a, b, c) SAED patterns corresponding to $La_{1/3}Sr_{2/3}FeO_{2.90}$ along the $[010]_c$ zone axis, for three different crystals.

on a JEOL 4000EX electron microscope, fitted with a double tilting goniometer stage (± 25°) by working at 400 kV. The samples were ultrasonically dispersed in *n*-butanol and transferred to carbon-coated copper grids.

RESULTS AND DISCUSSION

I. $La_{1/3}Sr_{2/3}FeO_{2.90}$

The XRD pattern can be indexed on the basis of a pseudocubic perovskite-type phase, although it was noted that the high angle peaks were somewhat broadened. The microstructural study developed by electron microscopy reveals, however, a more complex situation.

Figures 1a, 1b, and 1c show the SAED patterns along the $[010]_c$[2] zone axis, for three different crystals. Figures 2a and 2b correspond to the $[\bar{1}10]_c$ and $[1\bar{1}1]_c$ zone axes, respectively. In all cases, in addition to the diffraction maxima corresponding to the cubic subcell, some extra spots appear:

—In the $[010]_c$ zone axis it is possible to observe a group of four satellite reflections around the $(1/2\ 0\ 1/2)_c$ position in a cross-like disposition. Besides, two spots tripling one face diagonal of the basic cell appear. These features are present in all the crystals observed, although some differences in the relative intensities of the extra spots can be appreciated.

—By tilting 45° along c^*, the $[\bar{1}10]_c$ projection is obtained (Fig. 2a) showing two extra reflections at $(1/3\ 1/3\ 1/2)_c$ and $(2/3\ 2/3\ 1/2)_c$. Also a diffuse reflection doubling $[001]_c$ is observed and $[110]_c$ is tripled, as also shown in Fig. 1. Again, these extra features appear with different relative intensity from crystal to crystal.

—The $[1\bar{1}1]_c$ zone axis (Fig. 2b) shows a threefold superstructure along $[110]_c^*$ and equivalent directions.

[2] Subindex c refers to the basic perovskite subcell.

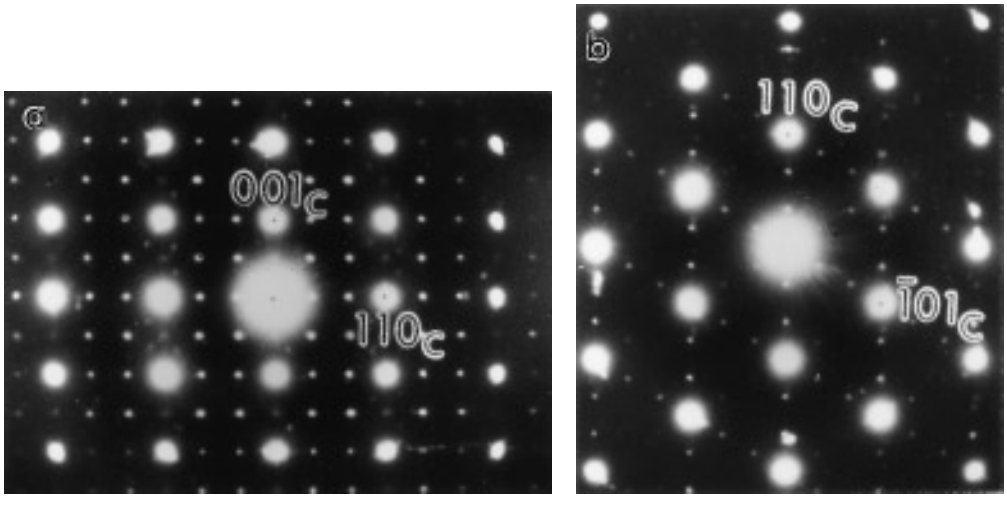

FIG. 2. SAED patterns for $La_{1/3}Sr_{2/3}FeO_{2.90}$ along the (a) $[\bar{1}10]_c$ and (b) $[1\bar{1}1]_c$ zone axis.

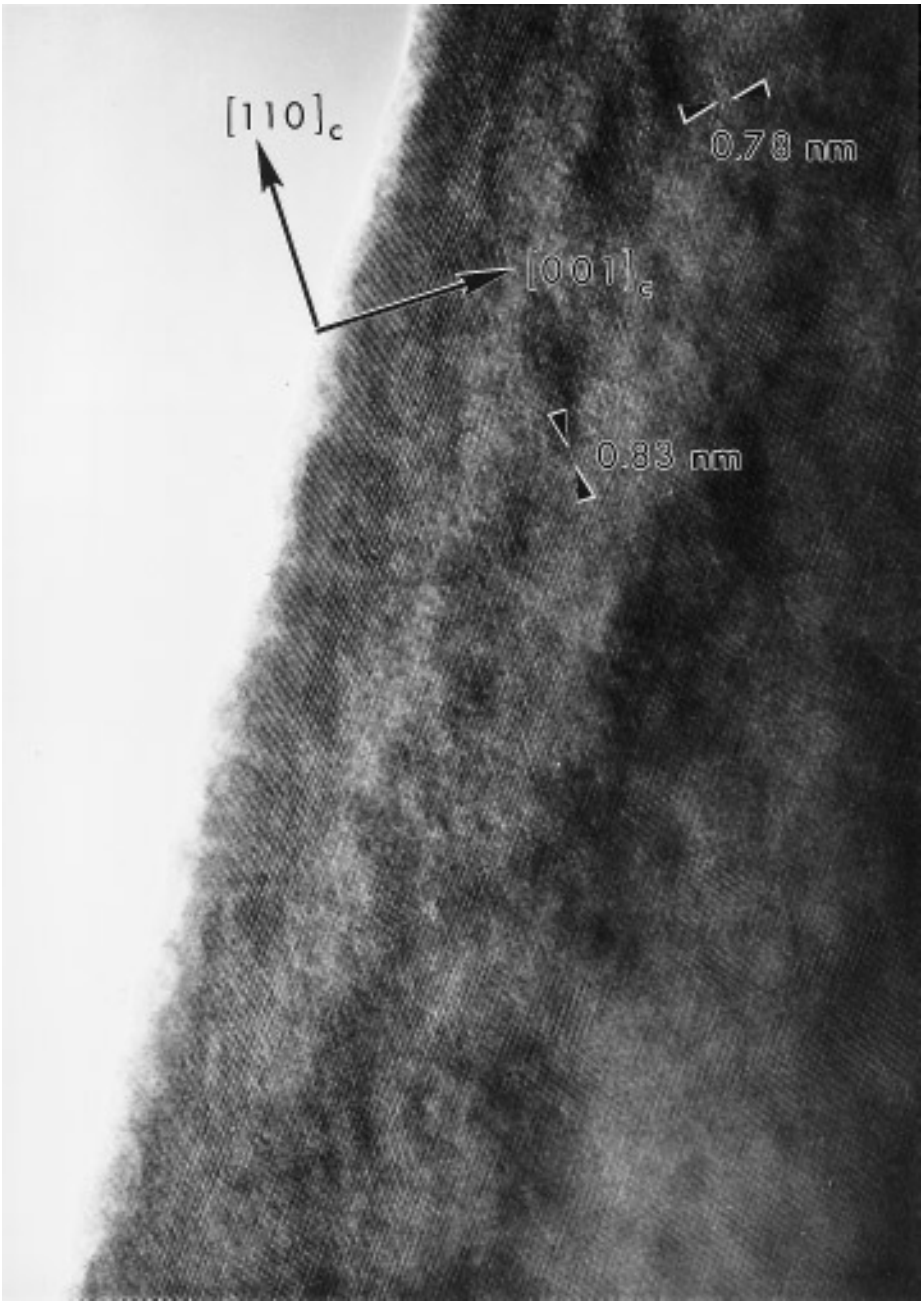

FIG. 3. High resolution electron micrograph for $La_{1/3}Sr_{2/3}FeO_{2.90}$ taken along the $[\bar{1}10]_c$ zone axis at low magnification. The presence of domains is evident.

The fact that the satellite spots are only visible by SAED and not by XRD should be related to a short range order situation and/or microdomain formation, which is also consistent with the appearance of the XRD pattern. The high resolution image shown on Fig. 3 corresponds to the $[\bar{1}10]_c$ zone axis; effectively, the presence of microdomains is evident. Some areas are visible where the $[110]_c$ direction is tripled and some others where $[001]_c$ is doubled. Lets analyze now the structural arrangement of each microdomain.

Figure 4 corresponds to an enlarged area of one of the domains shown before. Fringes along the $[334]_c$ direction are clearly seen. A careful examination of the image contrasts shows a twofold periodicity along the $[001]_c$ direction and a threefold periodicity along $[110]_c$ inside the domain. These contrasts are responsible for the satellite reflections

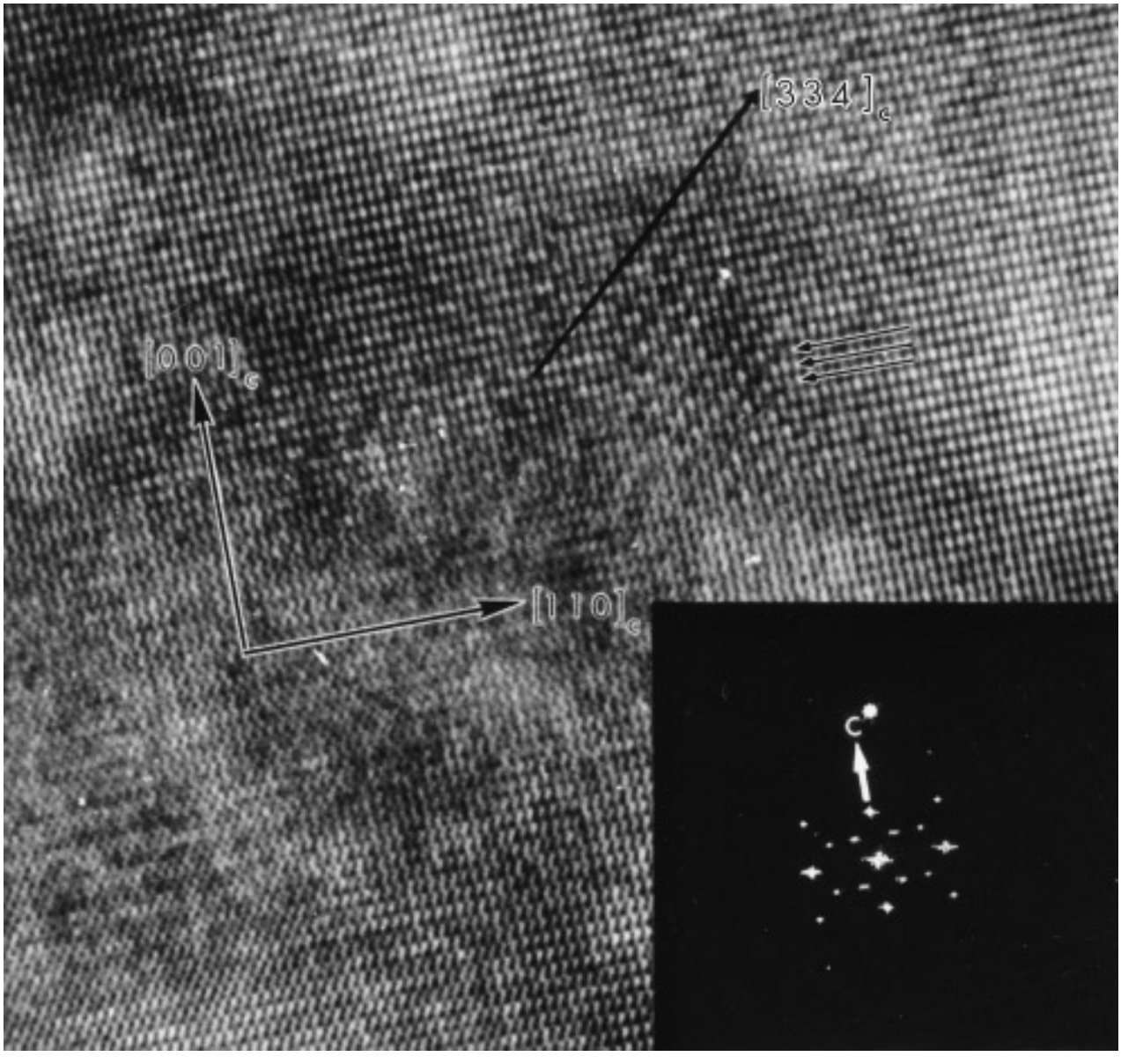

FIG. 4. Higher magnification of one of the domains shown in Fig. 3. The corresponding optical diffraction pattern can be seen in the inset. Arrows in the figure show the area where the optical diffraction has been performed.

at $(1/3\ 1/3\ 1/2)_c$ and $(2/3\ 2/3\ 1/2)_c$ as shown by optical diffraction (inset of Fig. 4). When tilting 45° along c* (Fig. 5), that is the $[010]_c$ zone axis, the domains are also visible. It is possible to observe contrasts tripling and doubling the $[100]_c$ and $[001]_c$ directions, respectively. This contrast variation leads to the appearance of fringes along the $[302]_c$ direction in this projection and it originates the satellite reflections forming two arms of the cross we mentioned before (see inset on Fig. 5). At this point, it is worth mentioning that the appearance of this kind of fringe is characteristic of a modulated structure. The distance between fringes along $[22\bar{3}]_c$ corresponds to $6 \times d_{223}$ (~5.7 Å). This distance coincides with the periodicity of the satellite reflections observed in the corresponding diffraction pattern (see inset of Fig. 4). In the same way, on the $[100]_c$ projection, the fringes periodicity along the $[20\bar{3}]_c$ direction is $6 \times d_{302}$ (~6.5 Å). Again, it corresponds to the satellite periodicity measured in the diffraction pattern on Fig. 5. To make the explanation easier, we have represented in a schematic way the contrast distribution in both projections (Fig. 6).

If we examine carefully the schematic distribution of contrasts in the $[\bar{1}10]_c$ projection there is a 2:1 ratio of strong and weak white spots along $[110]_c$, and the reverse

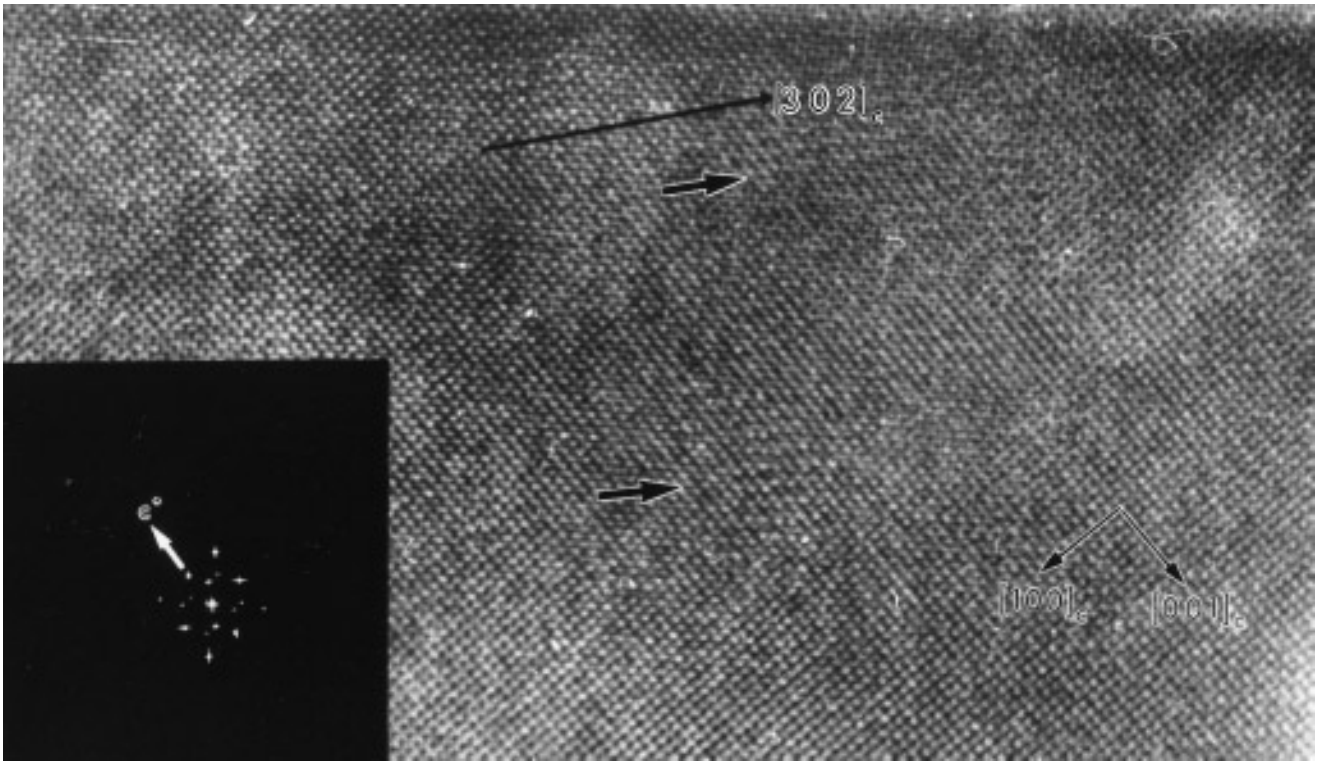

FIG. 5. High resolution image of $La_{1/3}Sr_{2/3}FeO_{2.90}$ along the $[010]_c$ zone axis. The corresponding optical diffraction pattern is shown in the inset. Arrows in the figure show the areas where the optical diffraction has been performed.

ratio contrast in the next plane, that is, doubling the $[001]_c$ direction. It gives rise to a periodicity of $3/2\sqrt{2}a_c$ along $[110]_c$. In the $[010]_c$ projection a similar change in contrast is observed along $[100]_c$ and again an alternance of strong and weak white spots occurs along $[001]_c$.

Previous studies on nonstoichiometry in AMO_{3-y} perovskites have clearly shown that the vacancy ordering is a function of y. In this sense, in cubic perovskite related ferrites, for y values below 0.15, the oxygen vacancies should be randomly distributed (12, 13). Both the chemical and thermogravimetric analysis have shown that the average oxyen composition leads to a relatively small amount of oxygen vacancies ($La_{1/3}Sr_{2/3}FeO_{2.90}$) and, therefore, a possible interpretation of the superstructure observed is a

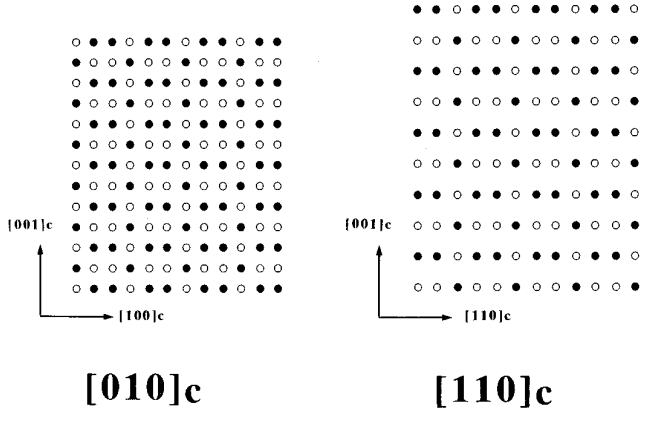

FIG. 6. Schematic representation of the contrast distribution observed in the experimental images shown in Figs. 4 and 5.

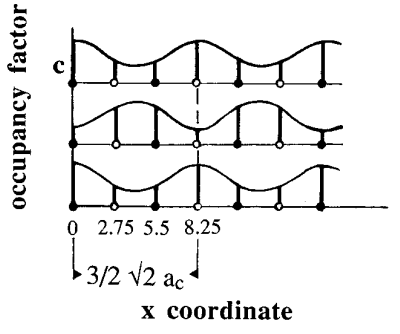

$$z=0 \qquad f(x) = 0.34 + 0.67\cos^2(\pi\, x/T)$$

$$z=1/2 \qquad f(x) = 0.34 + 0.67\,\mathrm{sen}^2(\pi\, x/T)$$

FIG. 7. Sinusoidal modulation along $[110]_c$ for the occupation factor of La and Sr in the A positions. Projection along the $[\bar{1}10]_c$ direction. Black and white circles correspond to Sr atoms at $y = 0$ and $y = 1/2$, respectively.

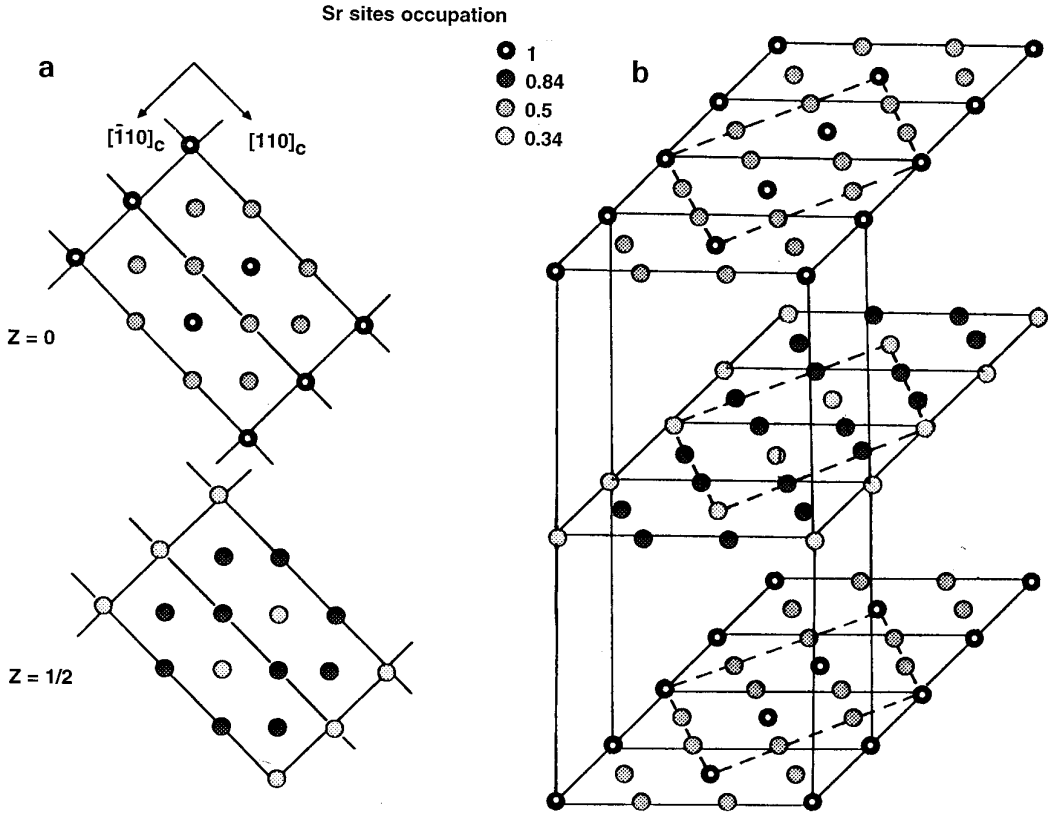

FIG. 8. (a) Schematic illustration of the $[001]_c$ planes at $z = 0$ and $z = 1/2$ where both Fe and O atoms have been omitted for simplicity. (b) Three-dimensional representation of the model proposed, showing the stacking sequence along *c*.

short range order situation involving Sr and La in the *A* positions.

Around each sharp reflection of the cubic subcell, only the first order satellites appear, suggesting a sinusoidal modulation affecting the occupation factor of La and Sr in the *A* sublattice. On a periodic distribution of atoms, a sinusoidal modulation of the atomic scattering factor leads to the appearance of first order satellites around each main reflection. The modulation period is obtained from the measurement of the distance between the main and the satellite diffraction maxima. In our case, this period is $3/2\sqrt{2}a_c$ along $[110]_c$.

Thus, the contrast observed in the HREM images on Figs. 4 and 5 can be interpreted as due to a compositional modulation affecting the occupation factor of La and Sr in the *A* positions. This modulation is described by a simple cosine function as

$$f(x) = A + B \cos^2 [(\pi/T)x + \Phi],$$

where, for the present case, x is the atomic coordinate for the *A* atoms along the $[110]_c$ direction, T is the modulation period ($T = 3/2\sqrt{2}a_c$), A, B are constants, and Φ is phase. According to the nominal composition, we introduce the limitation that the average occupation rate of Sr is 0.67 in every $(001)_c$ plane and 0.33 for the La atoms:

$$1/T \int_0^T f(x)\, dx = 0.67.$$

Figure 7 represents this sinusoidal modulation in a schematic way. The function was scaled to give a fully occupied Sr site at the origin of the unit cell. This occupation changes as a cosine function with a change in phase of $\pi/2$ from one $(001)_c$ plane to the next. Therefore, in the $(001)_c$ plane at $z = 1/2$, the origin is placed on one Sr atom with a minimum occupation rate.

Figure 8 corresponds to a schematic illustration of the $(001)_c$ planes at $z = 0$ and $z = 1/2$, where both the iron and oxygen atoms have been omitted for simplicity. The occupation factor of Sr on each position has been labeled and the difference to unity corresponds to La. From this interpretation we can describe a new cell of parameters $a_c\sqrt{2} \times a_c\sqrt{2} \times 2a_c$, with a modulation along [100] (or $[110]_c$) of period $T = 3/2\sqrt{2}a_c$.

The ideal atomic positions of *A* and *B* atoms with the corresponding occupation rate of Sr and La and without any restriction in symmetry (S.G. *P*1) have been used as

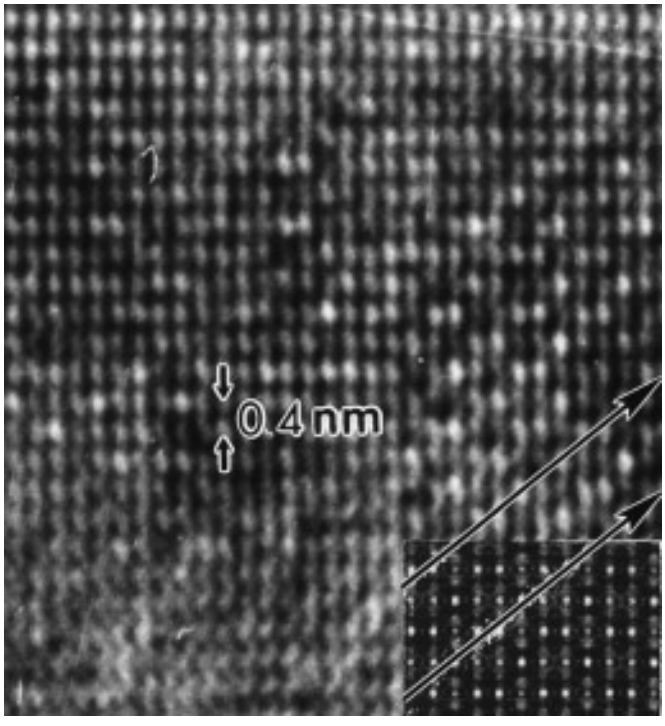

FIG. 9. Enlarged image of one domain in the $[\bar{1}10]_c$ projection. The simulated image is shown in the inset.

input data to simulate the changes in contrast observed in the HREM images [NCEMSS Program (14)]. In the $[\bar{1}10]_c$ projection, the agreement between the experimental and calculated images is satisfactory for a defocus value $\Delta f = -70.0$ nm and foil thickness $t = 4.5$ nm (Fig. 9). No major differences in contrast have been obtained when introducing oxygen atoms in the input data, which is reasonable if we think that, at this thickness, contrast in the images comes mainly from the heavy atoms. The oxygen atoms are usually neglected as weak scatters and their influence on the HREM contrast depends strongly on specimen thickness.

In the [100] projection, no imaging conditions (Δf, t) were found that could make it possible to distinguish the different occupation of Sr and La in the A positions. In the three-dimensional model represented in Fig. 8b, the cell along the $[100]_c$ viewing direction has been marked with dashed lines. As can be observed, the $\{100\}_c$ lattice plane spacings correspond to Sr/La atoms with different occupation rate, therefore the projected potential of the unit cell along this direction does not reflect the differences in contrast. However, the modulation is observed in the experimental image (Fig. 5), although the difference in contrast is less evident from the image features occuring in this projection than in the $[\bar{1}10]_c$ projection (Fig. 4). This fact suggests that the modulation affecting the occupation factor is accompanied by a displacive modulation (15). A refinement of the structural model proposed would lead to the atomic displacements, but the complex microstructure of this material makes the structural analysis very complicated.

II. $La_{1/3}Sr_{2/3}ReO_{3.00}$

As previously mentioned, this sample was prepared by annealing the $La_{1/3}Sr_{2/3}FeO_{2.90}$ sample under relatively high pressure of oxygen. Again, the XRD pattern shows all the diffraction maxima as corresponding to a simple cubic perovskite phase, but a sharpness of the peaks is clearly observed when comparing with the $O_{2.90}$ composition. From the electron diffraction study, the only extra feature with respect to the cubic subcell is a maximum doubling the $[111]_c^*$ reflection as it is observed in the SAED pattern taken along the $[\bar{1}10]_c$ zone axis (Fig. 10).

The existence of certain domains of a double perovskite phase in the crystals would be in agreement with this result. The fact that, according to the chemical and thermogravimetric analysis, we do not have oxygen vacancies at this composition implies that the doubling of the unit cell could be related to strontium–lanthanum 1 : 1 ordering in the A sublattice. This is likely associated to a Fe^{3+}–Fe^{4+} ordering provided that, for electrostatic reasons, those cations are also in a 1 : 1 ratio in the domains. The nondouble crystal regions should correspond to those where such order has not been established (16). In this way, the Sr/La ordering is such that each strontium atom is surrounded by lanthanum atoms and therefore, a La atom has Sr atoms as closest neighbors.

However, well ordered crystals are observed in the electron micrographs taken with beam incidence parallel to

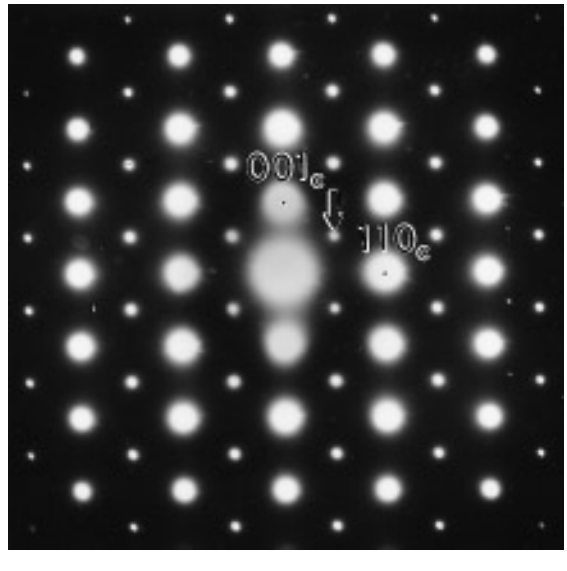

FIG. 10. Electron diffraction pattern corresponding to $La_{1/3}Sr_{2/3}FeO_{3.00}$ along the $[\bar{1}10]_c$ zone axis.

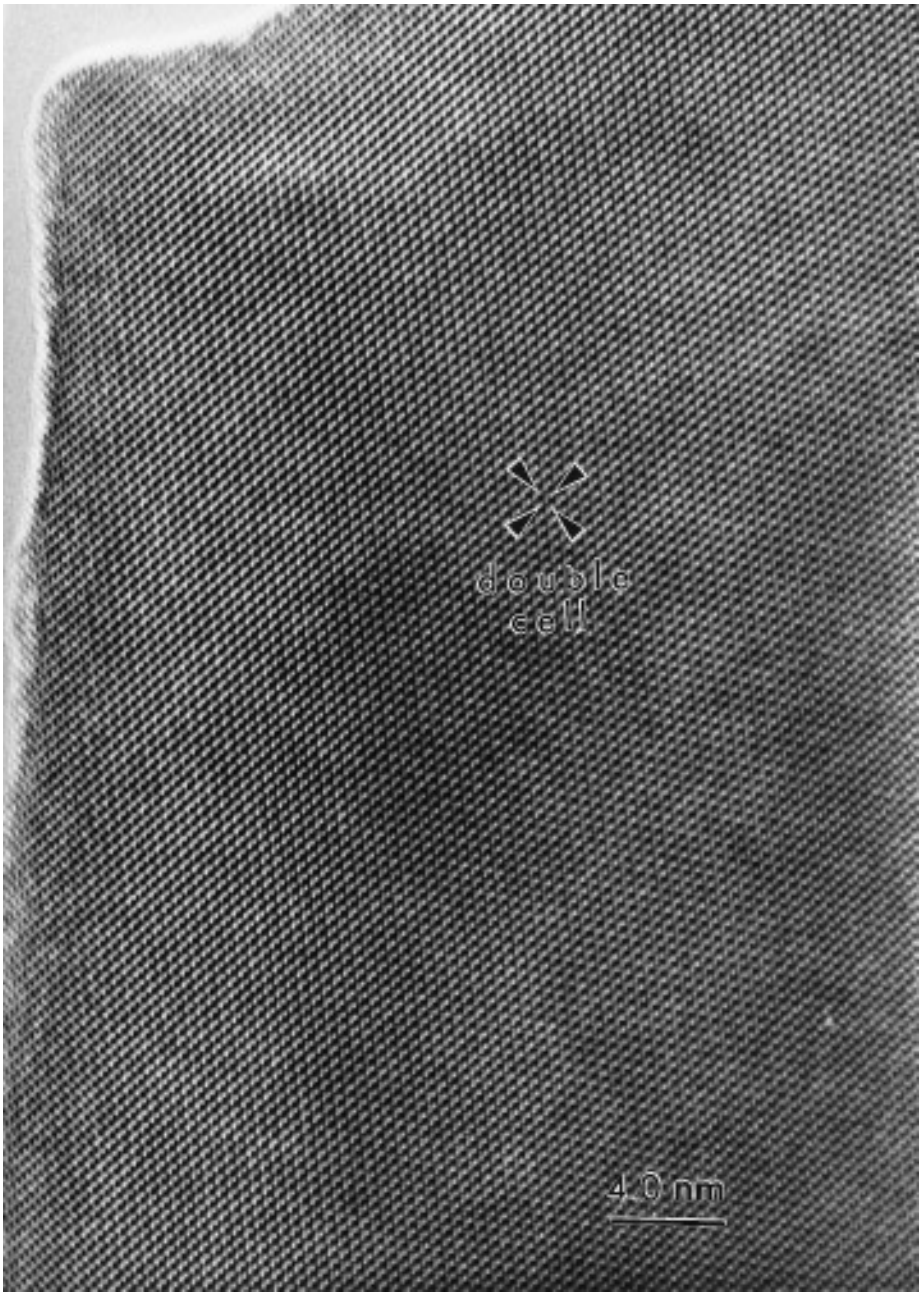

FIG. 11. High resolution electron micrograph corresponding to $La_{1/3}Sr_{2/3}FeO_{3.00}$ along the $[\bar{1}10]_c$ direction.

the $[\bar{1}10]_c$ direction, as shown in Fig. 11. Only the lattice fringes of the basic perovskite structure are revealed. An extensive study of several crystals of this sample does not show the presence of domains or any extended defect. Therefore, the hypothesis concerning ordering 1 : 1, Sr : La has to be rejected.

An alternative interpretation would imply the presence of a small distortion along one of the body diagonals of the aristotype cubic unit cell. This would preserve the 2 : 1,Sr : La cationic ratio. The rhombohedral distortion has been previously reported by Battle *et al.* (10) for the $La_{1/3}Sr_{2/3}FeO_{2.98}$ material by means of powder neutron diffraction data, the refinement parameters being a = 5.4712 Å, α = 60.09°, and space group $R\bar{3}c$. The corresponding hexagonal setting would be a 6H structural type with the c axis parallel to the $[1\bar{1}1]_c$ direction, in such a way that the $[\bar{1}10]_c$ projection would correspond to the [010] hexagonal projection. The maximum doubling the

$[111]_c^*$ direction can be indexed as the $(003)_h$ reflection. However, although only $(00l)$ reflections with $l = 6n$ are allowed, the $(003)_h$ maximum can appear as an effect of multiple diffraction.

The fact that the distortion is not observable by X-ray diffraction is consistent with the small angle deviation ($\alpha = 60.09°$), which could be detected by synchrotron radiation.

CONCLUSION

The microstructural study of the 1:2:3 compounds in the La–Sr–Fe–O system reveals that, for the $La_{1/3}Sr_{2/3}FeO_{2.90}$ material, La and Sr are ordered in small domains where the 1:2 ratio is preserved following a sinusoidal modulation. The presence of anionic vacancies favors the local ordering of the *A* sublattice and this short range order situation disappears when oxidizing the sample to $La_{1/3}Sr_{2/3}FeO_3$. For this anionic composition, the material undergoes a change to rhombohedral symmetry, the 1:2,La:Sr cationic ratio being preserved.

ACKNOWLEDGMENTS

This research was supported by C.I.C.Y.T. (Spain) through Projects MAT93-0207 and MAT95-0642. We thank the Centro de Microscopía Electrónica (U.C.M.) and specially to E. Baldonedo for facilities. We are also grateful to Dr. J. A. Alonso for valuable help in the high pressure synthesis.

REFERENCES

1. E. García-González, M. Parras, J. M. González-Calbet, and M. Vallet-Regí, *J. Solid State Chem.* **104,** 232 (1993).
2. E. García-González, M. Parras, J. M. González-Calbet, and M. Vallet-Regí, *J. Solid State Chem.* **105,** 363 (1993).
3. E. García-González, M. Parras, J. M. González-Calbet, and M. Vallet-Regí, *J. Solid State Chem.* **110,** 142 (1994).
4. J. C. Grenier, M. Pouchard, and P. Hagenmuller, "Structure and Bonding," Vol. 47, p. 1. Springer-Verlag, Berlin, 1981.
5. M. A. Alario-Franco, M. J. R. Henche, M. Vallet, J. M. González-Calbet, J. C. Grenier, M. Pouchard, and P. Hagenmuller, *J. Solid State Chem.* **46,** 23 (1983).
6. C. H. Yo, I. Y. Yung, K. H. Ryn, K. S. Ryn, and J. H. Choy, *J. Solid State Chem.* **114,** 265 (1995).
7. J. S. Waugh, M. I. T. Lab. for Insulation Res. Technical Report 152 (1960).
8. S. E. Dann, D. B. Currie, M. T. Weller, M. F. Thomas, and A. D. Al-Rawwas, *J. Solid State Chem.* **109,** 134 (1994).
9. P. D. Battle, T. C. Gibb, and S. Nixon, *J. Solid State Chem.* **77,** 124 (1988).
10. P. D. Battle, T. C. Gibb, and S. Nixon, *J. Solid State Chem.* **79,** 75 (1989).
11. P. D. Battle, T. C. Gibb, and P. Lightfoot, *J. Solid State Chem.* **84,** 271 (1990).
12. S. Komornicki, J. C. Grenier, M. Pouchard, and P. Hagenmuller, *Nouv. J. Chim.* **5,** 161 (1981).
13. J. M. González-Calbet, J. Alonso, and M. Vallet-Regí, *J. Solid State Chem.* **71,** 331 (1987).
14. NCEMSS Programm, National Center for Electron Microscopy, Material and Chemical Science Division, Laurence Berkeley Laboratory, University of California, Berkeley, California 1989.
15. A. Guinier, "Théorie et Technique de la Radio-Cristallographie, Chapitre XIII." Dunod, Paris, 1964.
16. M. Vallet-Regí, E. García, and J. M. González-Calbet, *J. Chem. Soc. Dalton Trans.* **3,** 775 (1988).